Journal of Materials Chemistry A

PAPER

View Article Online
View Journal | View Issue

Cite this: J. Mater. Chem. A, 2018, 6, 266

Particle and nanofiber shaped conjugated microporous polymers bearing hydantoin-substitution with high antibacterial activity for water cleanness†

Fei Wang, [a] Feng Ren, [a] Dan Ma,[a] Peng Mu, [a] Huijuan Wei,[a] Chaohu Xiao, [ab] Zhaoqi Zhu,[a] Hanxue Sun, [a] Weidong Liang, [a] Jixiang Chen,[a] Lihua Chen*[b] and An Li *[a]

Efficient elimination of widespread microbial contamination in water is of great importance to address severe environmental issues. Herein, we demonstrate a new strategy for fabricating novel CMPs-based antibacterial agents by covalently introducing hydantoin groups into CMPs networks (named as CMPH). The resulting CMPH show excellent physicochemical stability, large specific surface areas (up to 1411 m^2 g^{-1}) and high antibacterial activity (completely inhibiting growth of bacteria at 100 μg mL^{-1} dispersion concentration in 120 min). To our knowledge, this is the first example of a CMPs-based antibacterial agent. Furthermore, the CMPH can not only be fabricated as monolithic nanoporous foam, but also can be loaded on diverse porous substrates to fabricate cost-effective sterilization materials, showing great potentials for their practical applications in water cleanness. More importantly, the findings of this study may open a versatile route for design and fabrication of CMPs-based antibacterial materials by the facile introduction of diverse of antibacterial substituents into CMPs building blocks followed by a simple one-pot reaction.

Received 25th October 2017
Accepted 28th November 2017

DOI: 10.1039/c7ta09405a

rsc.li/materials-a

Introduction

Microbial contamination gradually became a main route of transmission of infectious diseases,[1–6] and generally these contaminations have good solubility in water and can penetrate to deep soil strata and reach groundwater.[7] Vast economic losses and death caused by infectious diseases originating from microbial contaminants in polluted water has been a major issue hindering social development, especially for those in underdeveloped areas. In a classical sterilization process, chlorine gas, chlorine dioxide gas, and ozone gas are the most efficacious disinfectants for killing most microorganisms, but these methods have limitations of the undesirable property of being toxic gases at ambient temperatures which are thus potential hazards to operation workers and they may lead to other environmental risks as well.[8] Hence, the development of new and high performance water disinfectants still remains a big challenge for public health control of emerging infectious diseases, especially for water polluted with microbial contaminants.

Generally speaking, antibacterial mechanisms are classified as follows: organic molecules with positive charge bind to the negative charge on the microbial cell membrane, or damage the cell wall permeability thus leading to the loss of life-sustaining nutrients or reducing their intake, or they enter the cell and react with cell substances to interfere with cell metabolism. Accordingly, diverse kinds of antibacterial agents with antibacterial active sites or groups have been created to meet the emerging demand for purification of water; these include hydantoin,[9] *N*-halamine-based polymers,[10] graphite,[11] graphite oxide (GO),[11] graphene oxide, reduced graphene oxide (rGO) and carbon nanotubes (CNTs),[12–15] *etc.* For GO and rGO, the antibacterial activities have been attributed to membrane stress induced by sharp edges of graphene nanosheets, which may result in physical damages on cell membranes, leading to the loss of bacterial cell membrane integrity and the leakage of RNA.[11,13] The antibacterial activity of CNTs has been found to have the synergy of both "physical" and "chemical" effects. When bacteria directly contact with CNTs, intensive physical interactions between CNTs and bacterial cells may cause physical damages on cell membranes, and result in the release of intracellular contents.[11,14,15]

[a]College of Petrochemical Technology, School of Material Science and Engineering, Lanzhou University of Technology, Lanzhou 730050, P. R. China. E-mail: lian2010@lut.cn

[b]Experimental Center, Northwest Minzu University, Lanzhou 730030, P. R. China. E-mail: clh@xbmu.edu.cn

† Electronic supplementary information (ESI) available. See DOI: 10.1039/c7ta09405a

Compared with those carbon-based antibacterial agents, *N*-halamine containing compounds or polymers show better antibacterial activity and the biocidal mechanisms of *N*-halamine can be classified into contact killing, release killing, and transfer killing.[10,16,17] From a practical point of view, *N*-halamine containing polymers or polymers bearing *N*-halamine substituents are more suitable for their antibacterial operation in comparison with the direct use of *N*-halamine containing compounds in water. For fabrication of such *N*-halamine containing polymeric materials, the covalent introduction of *N*-halamine structures into a number of polymer substrates is a popular approach. In most cases, however, such approach suffers the drawbacks of either being difficult to perform because of the chemical inertness of polymeric substrates or deterioration of the physical properties of the polymers and/or complicating the fabrication processes of the final products.[18–20] Therefore, the exploitation of new approaches for construction of antibacterial agents is of special interest.

Hydantoin compounds are a kind of five membered heterocyclic compounds containing various substituents, and their derivatives have lots of applications, such as a vitro inhibitor,[21–23] antiviral,[24,25] anti-inflammatory agents,[26] glucokinase activators,[27] sodium channel blockers,[28] *etc.* As a kind of precursor for synthesis of *N*-halamine compounds, hydantoin itself has widely been used as an antibacterial agent. In this work, we demonstrate a novel strategy for fabrication of hydantoin-based antibacterial agents by covalent introduction of hydantoin groups into the skeleton of three-dimensional (3D) conjugated microporous polymer (CMPs) networks (named as CMPH). Compared with those well-studied nanoporous materials such as metal–organic frameworks (MOFs) and covalent organic frameworks (COFs) usually having uniform and defined microporous architectures formed in crystalline structure,[29–32] CMPs have amorphous porous and rigid π-conjugated structures, larger surface areas, and high thermal and chemical stability, which have been the subject of much interest in a wide range of applications.[33–46] The primary design for our strategy takes great advantage of designable flexibility of the CMPs materials which allows us to endow the antibacterial functionality for CMPH only by employing bromo-substituted hydantoin and alkynyl benzene as monomers *via* a simple, one-pot Sonogashira–Hagihara cross-coupling condensation reaction. As a proof-of-concept study, two CMPH with high antibacterial activity and large specific surface areas up to 1411 $m^2\ g^{-1}$ have been developed in this study. The as-prepared CMPH shows high thermal and chemical stability which rend the materials to withstand harsh environmental conditions. To the best of our knowledge, this is the first example of covalently employing CMPs as a substrate to fabricate such antibacterial agents. In addition, the CMPH can not only be fabricated as a monolithic nanoporous foam, but also can be loaded on the surface of diverse porous substrates such as filter paper, cloths and even sponges, showing great potential for their practical applications as an efficient antibacterial agent in water in various operation manners.

Results and discussion

We designed and fabricated these novel antibacterial agents by covalent incorporation of a hydantoin moiety (acts as antibacterial active site) into a CMPs skeleton. To this end, CMPH-1 was synthesized using 1,3-dibromo-5,5-dimethylhydantoin (DBDMH) and 1,3,5-triethynylbenzene (abbreviated as A) as monomers by a palladium-catalyzed Sonogashira–Hagihara cross-coupling reaction. Additionally, CMPH-2 was synthesized using DBDMH and 1,4-diethynylbenzene (abbreviated as B) as monomers by the same method as that of CMPH-1. As shown in Scheme 1, CMPH were constructed with two different 3D architectures of A2B3 type for CMPH-1 and A2B2 type for CMPH-2, respectively. The simulation structure of CMPH-1 shows that it has a three-dimensional network structure, while CMPH-2 exhibits a twist cylindrical architecture. Such differences arising from the molecular structure of ethynylbenzene monomers would lead to the diversification in morphology of CMPH samples which are presented below (see Fig. 4a–d).

The molecular level structures of CMPH were investigated by ^{13}C solid-state NMR measurements, and ^{13}C CP/MAS NMR spectra of CMPH are shown in Fig. 1. Carbon atoms in different chemical environments corresponding chemical shifts are used to assign the peaks. Chemical shifts of CMPH-1 and CMPH-2 are basically similar. The observed appearance of resonance at $\delta = 25$ ppm can be assigned to the $-CH_3$ site. The resonance at $\delta = 59$ ppm can be ascribed to sp^3 carbons in the five-membered heterocyclic ring. The peaks centered around 78 ppm and 88 ppm can be assigned to –C≡C– units. The peaks at *ca.* 122 ppm and 132 ppm are observed for protonated and non-protonated C_{Ar} sites, respectively. The peaks close to 159 ppm and 180 ppm are ascribed to C=O sites.

The FTIR spectra of CMPH-1 and CMPH-2 are shown in Fig. 2a. It can be seen that most of the fingerprint peaks of the monomer remain in its polymers (Fig. 2a), and the main adsorption peaks of the two polymers (CMPH-1 and CMPH-2) are basically similar; the pit-like peak at *ca.* 3450 cm^{-1} can be ascribed to –OH stretching vibration of physisorbed water by

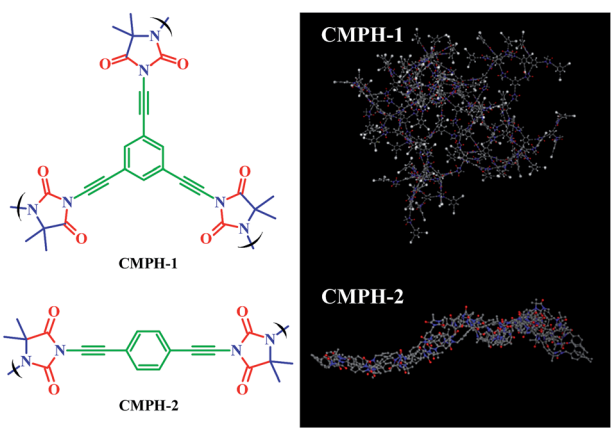

Scheme 1 Molecular structural formula and simulation structure of CMPH-1 and CMPH-2 (Materials Studio, polymer builder).

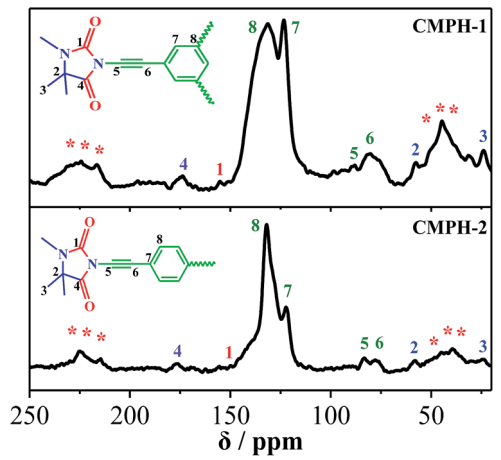

Fig. 1 ^{13}C CP/MAS NMR spectra of CMPH-1 and CMPH-2.

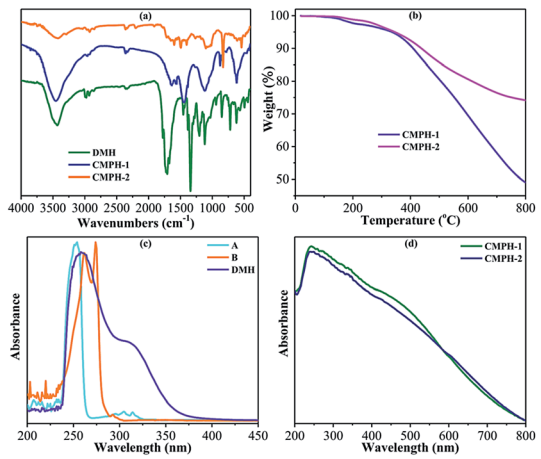

Fig. 2 (a) FTIR spectra of CMPH-1 and CMPH-2, (b) TGA curves of CMPH-1 and CMPH-2, (c) UV-vis adsorption spectra of A (1,3,5-triethynylbenzene), B (1,4-diethynylbenzene), and DMH, (d) solid UV-vis adsorption spectra of CMPH-1 and CMPH-2.

the polymers,[47] the characteristic peaks of –CH_3 at 2961 cm^{-1}, 1450 cm^{-1}, and 1380 cm^{-1} can be assigned to the symmetrical stretching vibration of C–H, symmetric bending vibration of C–H, and in-plane bending vibration of C–H, respectively. For CMPH-2, the weak peak appearing at 2200 cm^{-1} was attributed to –C≡C– stretching.[47,48] While for CMPH-1, the peak at 2200 cm^{-1} is too weak to be observed due to the symmetrical molecular structure of the A monomer. Also, the absorption peak at *ca.* 1650 cm^{-1} is the characteristic peak of the amide, which refers to the C=O stretching vibration. Apparently, the benzene ring has two adsorption bands: the first absorption band at 1650–1450 cm^{-1}, due to benzene stretching,[49] while a second absorption band appeared at 900–600 cm^{-1}, which can be assigned to skeleton vibration of the benzene ring. Moreover, it is worth mentioning that the characteristic peak at 900–600 cm^{-1}, which refers to substitution of a benzene ring, was observed. And the absorption peaks of the aromatic ring substitution present red shifts due to enhancing of the conjugation structure of the two polymers.[50] For CMPH-1, peaks appearing at 849 cm^{-1} and 781 cm^{-1} were attributed to the Ar–H bending vibration of a three-substituted ring. For CMPH-2, the adsorption band at 831 cm^{-1} is attributed to the Ar–H stretching vibration of *p*-substituted phenyl.

The thermal stability of CMPH-1 and CMPH-2 samples was investigated by TGA. As shown in Fig. 2b, the two polymers exhibit a very small weight loss below 150 °C, implying a loss of moisture. The decomposition temperature of CMPH-1 is 350 °C, indicating that the oxygen-containing group (carbonyl group) of CMPH-1 was removed to some extent. And the major weight loss for CMPH-1 at 550 °C is due to decomposition of the cross-linked polymer network, where the weight loss is 25 wt%. For CMPH-2, the thermal decomposition temperature is beyond 350 °C and the main weight loss of 18 wt% was found to be at 550 °C. The thermal stability of CMPH-2 is thus much better than CMPH-1, which may be attributed to the fewer oxygen-containing groups and low conjugated structures of CMPH-2. Compared with those linear polymers used as substrates for grafting-on the antibacterial active substituents, which usually suffer from low thermal stability, the rigid π-conjugated structure endows the as-synthesized CMPH samples high thermal stability which may be beneficial to their practical applications and also satisfied our primary design.

UV-vis spectra were measured to further confirm the polymerization degree of CMPH. As shown in Fig. 2c and d, three monomers have strong absorption at 250 nm. For compounds A and B, the main absorption band is concentrated at 250–275 nm, which is due to the alkynyl (chromophone) directly attached to the benzene ring. While for DMH, the low-intensity absorption band at 309 nm is ascribed to the –Br (auxochrome) directly connected to the conjugated system. The wavelength of the CMPH, as compared with the monomer, is longer (shown in Fig. 2d) due to the significant increase in conjugation length.[50]

The porosity of CMPH-1 and CMPH-2 was evaluated by nitrogen gas adsorption and desorption measurement at 77 K. As shown in Fig. 3a, both of the polymers give rise to type-II/IV mixed nitrogen gas sorption isotherms with H3 hysteresis loops,[51] indicating the existence of mesopores and macropores in the resulting polymers, which can be further proven by analyzing their pore size distribution (PSD) curves (shown in Fig. 3b). As shown in Fig. 3b, both CMPH-1 and CMPH-2 mainly contain mesoporosity and the adsorption average pore width was calculated to be 27 nm for CMPH-1 and 38 nm for CMPH-2, respectively. The apparent BET surface areas and total pore

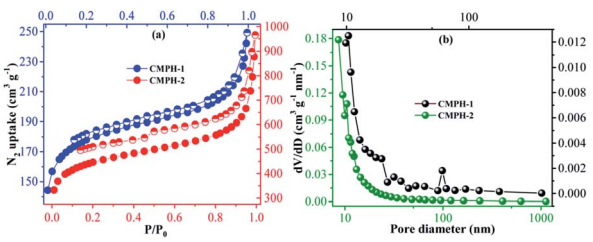

Fig. 3 (a) Nitrogen adsorption–desorption isotherms of CMPH-1 and CMPH-2 and (b) BJH pore size distribution curves of CMPH-1 and CMPH-2.

volumes were found to be 549 $m^2\ g^{-1}$ and 0.375 $cm^3\ g^{-1}$ for CMPH-1 and 1411 $m^2\ g^{-1}$ and 1.358 $cm^3\ g^{-1}$ for CMPH-2, respectively. The experimental data are also summarized in Table S1.† In most cases the antibacterial active substituents, *e.g.*, *N*-halamine,[16,52] were grafted on the linear polymers or textile which have poor surface areas; however, our CMPH materials take great advantage of both large surface areas and pore volumes which may facilitate polluted water to adequately access the active sites of the CMPH network. On the other hand, to the best of our knowledge, the grafting of antibacterial active substituents onto such porous substrates for construction of antibacterial agents has rarely been reported previously.

Fig. 4 shows the SEM images of CMPH-1 and CMPH-2, respectively. Interestingly, the two samples exhibit totally different morphologies even though they have similar chemical constituents. In the case of SEM images, the sample of CMPH-1 is composed of smooth and aggregated polymeric spheres with diameters in the range of 500–900 nm (Fig. 4a and b). In contrast, CMPH-2 consists of fiber-like morphology and the diameters of the nanofibers are estimated *ca.* 200 nm (Fig. 4c and d). In fact, tuning of morphology of CMPs for synthesis of low-dimensional solids by varying the strut length of monomers has been well investigated in our previous studies.[53–59] In particular, we believe that the CMPH-2 nanofibers may have better processability for practical application purposes compared with those CMPs usually formed as unprocessable powders.

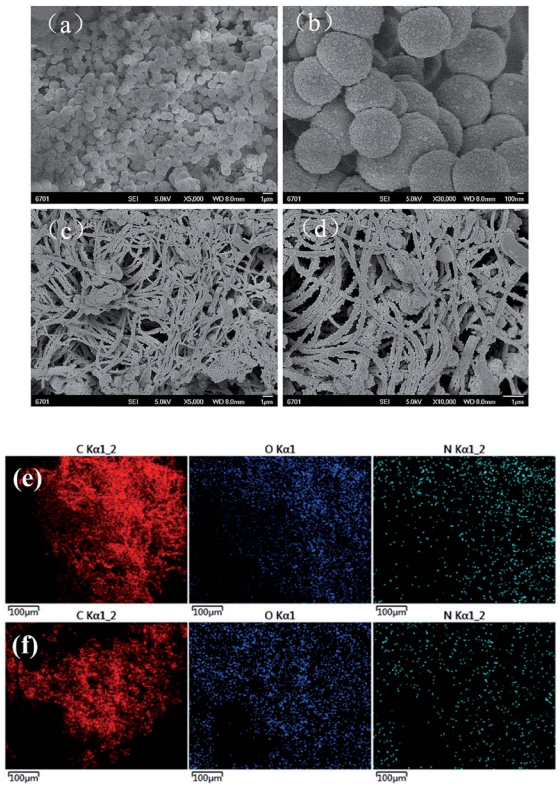

Fig. 4 SEM images of (a, b) CMPH-1 and (c, d) CMPH-2. Scale bar: 1 μm for (a, c, d) and 100 nm for (b), SEMEDX images of (e) CMPH-1 and (f) CMPH-2.

In order to further confirm the existence of hydantoin functional groups, which can inhibit the growth of bacteria, scanning electron microscopy with energy dispersive X-ray (SEMEDX) analysis was utilized to determine chemical compositions of the polymers. As shown in Fig. 4e and f, the polymers (CMPH-1 and CMPH-2) dominantly consisted of carbon (C), oxygen (O), and nitrogen (N) elements. The overwhelming content of C and the little content of O and N are consistent with the sketches of the polymers (shown in Scheme 1) and the uniform distribution of O and N, which is beneficial for a bacteriostatic experiment.

Elemental analysis was conducted to further investigate the accurate content of the functional groups in the CMPH and the results are summarized in Table S2.† The contents of C, H, and N were measured to be 76.7 wt%, 3.9 and 2.6 for CMPH-1 and 82.9 wt%, 3.9 and 2.8 for CMPH-2, respectively. These results, obtained by combination of elemental analysis and SEMEDX, are in good agreement with ^{13}C CP/MAS NMR spectra and FTIR spectra which further confirmed the chemical constitution and structure of CMPH samples.

Based on the outstanding physicochemical stability and their unique functional groups, the resulting polymers should be a kind of good bacteriostatic agent. *E. coli* and *S. aureus* were used as model bacteria to evaluate the antibacterial activities of our materials. We also employed 5,5-dimethylhydantoin (DMH) monomer, which has widely been used as an antibacterial agent, as a control. As shown in Fig. 5, under same concentration and incubation conditions, CMPH-1 shows the highest antibacterial activity, sequentially followed by CMPH-2 and DMH. Notably, given a dispersed concentration of CMPH-1 of 100 μg mL^{-1}, the growth of *E. coli* could be inhibited completely in 2 hours. Clearly, the CMPH samples have better antibacterial activity than that of DMH. It is suggested that the hydantoin active sites in the CMPH network along with the inherent physicochemical properties of CMPs should be responsible for such excellent antibacterial activity. As a proof-of-concept study, these results are well consistent with our preliminary design.

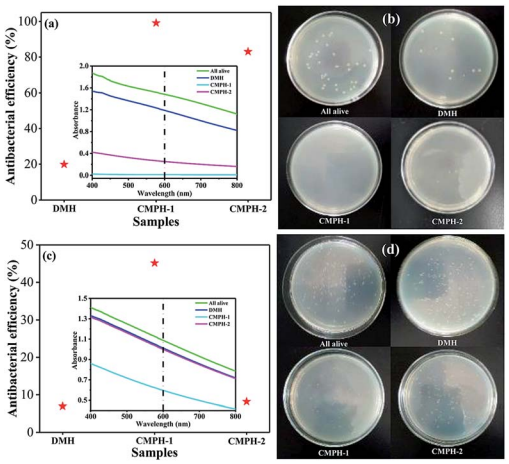

Fig. 5 Antibacterial activity of DMH and CMPH for (a) *E. coli* and (c) *S. aureus* and antibacterial assay in Petri dishes: (b) *E. coli* and (d) *S. aureus* incubated with LB.

According to previous studies,[17] the antibacterial mechanism of the N–O moieties (*e.g.*, *N*-halamine compounds and hydantoin compounds) can be classified into contact killing, release killing, and transfer killing.

In this regard, X-ray photoelectron spectroscopy (XPS) spectra were measured using CMPH-1 to further investigate such an antibacterial mechanism. As shown in Fig. 6, for the samples untreated with CMPH-1, the peaks at 399.9 eV and 532.4 eV are assigned to N and O species of hydantoin moieties in the CMPH structure. After antibacterial treatment, the peaks for N and O remain unchanged, indicating there are no changes in valence states of N and O observed before and after antibacterial treatment. Therefore, the hydantoin groups in CMPs networks remain stable during the whole antibacterial treatment. According to the above three antibacterial mechanisms as ascribed in previous studies,[60] the release killing and transfer killing are not a likely mechanism for antibacterial action owing to the stable hydantoin groups. In combination with previous studies, and based on the unique chemical structure of our materials, it is suggested that contact killing may be the main mechanism for antibacterial action.

The procedure for antibacterial activity of CMPH is schematically shown in Fig. 7a. As can be seen, when the living bacteria (blue for *E. coli* and golden for *S. aureus*) were contacted with the hydantoin moieties, permeability of the cell membrane would be changed, thus resulting in the death of bacteria (white). To investigate the morphology of bacteria before and after CMPH treatment, SEM for *E. coli* on the CMPH samples were conducted and results are shown in Fig. 7b, c and d. As can be seen in Fig. 7b, the cells without contacting the CMPH were intact and maintained their outer membrane structure. After contacting with the CMPH-1 (Fig. 7c and d), the cells had lost their cellular integrity and had become elongated and rough, indicating irreversible cell damage or cell death.

We also systematically investigated optimal antibacterial activity of the CMPH samples under different experimental conditions. The time-concentration dependent antibacterial behavior of CMPH were examined to evaluate their performance (Fig. 8). *E. coli* cells and *S. aureus* cells were incubated with various concentrations (50, 100, 250, and 500 μg mL^{-1}) of CMPH-1 and CMPH-2 dispersions in double distilled water for 60 min, 120 min, 180 min, and 240 min, respectively. As shown in Fig. 9, the loss of bacteria viability progressively goes up with

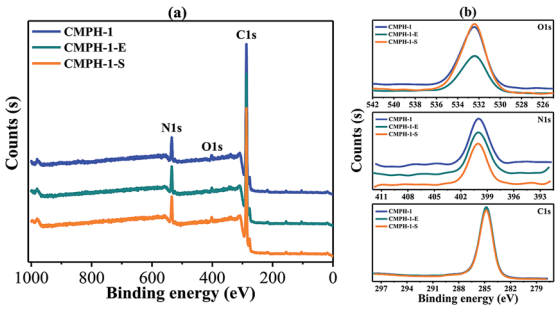

Fig. 6 XPS spectra of CMPH-1 (a) overall spectra and (b) single element spectra.

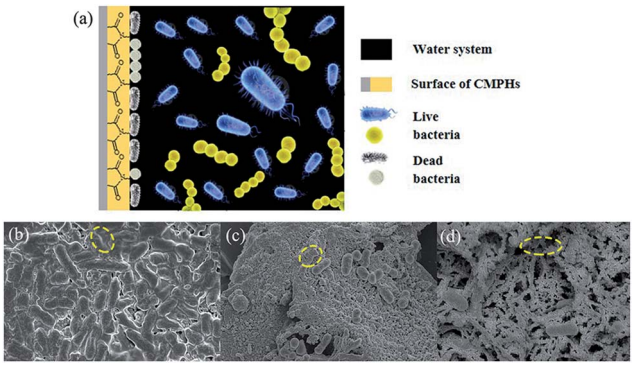

Fig. 7 (a) Schematic illustration for antibacterial mechanism of CMPH and SEM images of (b) *E. coli* and *E. coli* contact with the (c) CMPH-1 and (d) CMPH-2.

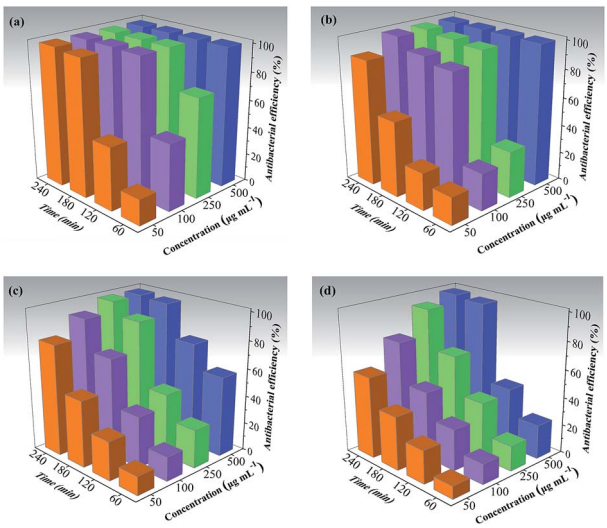

Fig. 8 The time–concentration dependent antibacterial activity of CMPH-1 for (a) *E. coli* cells and (b) *S. aureus*, and CMPH-2 for (c) *E. coli* cells and (d) *S. aureus*.

increases of CMPH concentration and antibacterial duration. The loss of *E. coli* viability jumps from 19.59% at the CMPH-1 concentration of 50 μg mL^{-1} to 100 at 500 μg mL^{-1} in an hour. While for *S. aureus*, the loss of *S. aureus* viability increases from 13.58% at CMPH-1 concentration of 50 μg mL^{-1} to 57.38% at 500 μg mL^{-1} in an hour. CMPH-2 dispersion displays a similar trend. The loss of bacteria viability was counted at hourly intervals. The loss of *E. coli* viability increased from 19.59% after 60 min to 45.43% after 120 min, and further increased to 98.32% after 180 min and 100% after 240 min at the CMPH-1 concentration of 50 μg mL^{-1}. And the loss of *S. aureus* viability was 18.65%, 27.91%, 47.86% and 79.89% after 60 min, 120 min, 180 min, and 240 min, respectively. These results suggest that the antibacterial activity of CMPH-1 dispersion has much higher antibacterial activities than CMPH-2 dispersion for *E. coli* cells and *S. aureus* in all experiments. CMPH-1 can completely inhibit the growth of *E. coli* in 2 h at a concentration of 100 μg mL^{-1}; this value has comparability with GO (95%) and

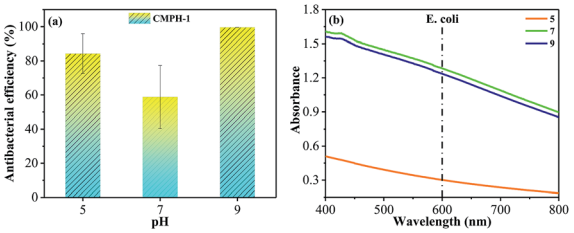

Fig. 9 (a) Antibacterial activity of CMPH-1 for *E. coli*, (b) the growth of *E. coli* at different pH.

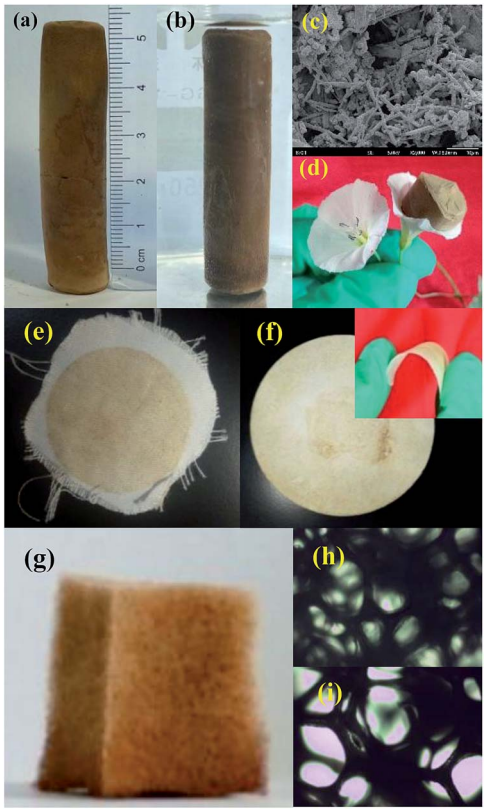

Fig. 10 The camera picture of (a) monolithic CMPH-1 foam (1 cm in diameter and 5 cm in length) and (b) the direct application of CMPH-1 for sterilization in water, (c) SEM images of CMPH-1 showing a porous 3D networks structure, (d) CMPH-1 foam was placed on the top of a flower showing its light weight nature, (e) loading of CMPH-1 into cloths and (f) filtration paper to prepare membrane-like antibacterial materials, (g) CMPH-1 was loaded onto the skeleton of a common polyurethane sponge using the PDMS as an adhesive layer, (h) optical camera pictures of untreated sponge, and (i) a CMPH-1 loaded sponge.

rGO (80%),[11] but is much higher than hydantoin (20%). And the minimum inhibitory concentration of CMPH-1 at 100 μg mL^{-1} is higher than AcOH(acetic acid) 0.25 wt% (2500 μg mL^{-1}), chitosan (250 μg mL^{-1}) and DEMC (125 μg mL^{-1}).[61]

Based on increasingly serious water pollution and complex water systems, antibacterial functions of the polymers were conducted at different pH values. As we all know, pH is an important factor on strain growth; both alkaline and acidic conditions affect the growth of bacteria, and the optimum growth pH of most bacteria is 6.5–7.5 although some also can live at 4.0–10.0. For our experiments, the optimum growth pH of *E. coli* and *S. aureus* was 7.2–7.6. We measured the antibacterial functions of CMPH-1 for *E. coli* at different pH of 5, 7, and 9 (shown in Fig. 9), and found that the acidic environment has a great impact on the growth of bacteria, but an alkaline environment had a better antibacterial effect. Bacterial proteins carry more negative charges in a neutral or alkaline environment, which can enhance the interaction with positively charged CMPH, and influence the permeability of a bacterial cell membrane, disrupting their metabolism, and finally leading to cell death.

In addition to excellent antibacterial activity, the as-prepared CMPH samples have good processibility for practical applications. As shown in Fig. 10, for example, the nanoporous foam of CMPH-1 can be synthesized by a facile tuning of the molar ratio of monomers. As a monolithic material, the nanoporous foam of CMPH-1 can be directly used in water cleanness (Fig. 10a), which has great advantages over those CMPs usually formed as unprocessable powders. The monolithic CMPH-1 foam is very light in weight and it even can be placed on the top of a flower without exerting an external force (Fig. 10d). To our knowledge, unlike those CMPs usually formed as unprocessable powders, such a monolithic form of CMPH has rarely been reported which can be directly used without further processing. The CMPH samples can be loaded into filter paper or cloths as filtering sterilization materials similar to commercial membranes (Fig. 10e and f). More interestingly, the CMPH samples can also be loaded on low cost and macroscopically porous substrates to fabricate an antibacterial agent (Fig. 10g). In this case, CMPH-1 can be coated into a polyurethane sponge utilizing polydimethylsiloxane (PDMS) as adhesive by a simple dipping coating method. Such formation diversity of CMPH samples makes it possible to process the CMPH in different manners to meet various application demands, thus showing great potential for real water cleanness.

Experimental

Materials

1,3,5-Triethynylbenzene (abbreviated as A) and 1,4-diethynylbenzene (abbreviated as B) were purchased from TCI. Copper(I) iodide and tetrakis(triphenyl-phosphine)palladium(0) were provided by J & K, and 1,3-dibromo-5,5-dimethylhydantoin (DBDMH) was obtained from Aladdin. All other regents were of analytical grade and used without additional purification.

Synthesis of hydantoin-based CMPs

The target products were synthesized *via* a palladium-catalyzed Sonogashira–Hagihara cross-coupling condensation reaction of alkynyl benzene and bromated hydantoin. In a classical synthetic technique, the molar ratio of alkynyl and bromine is 1 : 1. A (2 mmol), DBDMH (3 mmol), tetrakis(triphenyl-phosphine)palladium(0) (100 mg), and copper(I) iodide (40 mg) were dissolved in a mixture of toluene (7 mL) and Et_3N (7 mL) under nitrogen gas protection. The mixture was heated and

kept at 80 °C for 72 h with magnetic stirring. Then it was cooled to room temperature, filtered, and washed with dichloromethane, acetone, water, and methanol one by one to remove any unreacted monomers or catalyst residues. Soxhlet extraction with methanol for 72 h was carried out to make the crude product pure. The resulting product was dried at 60 °C to produce an insoluble solid. The solids were named as CMPH-1 and CMPH-2 for the different alkynyl monomers.

Preparation of various shaped CMPH

For preparing CMPH foam, the molar ratio of alkynyl and bromine is 3 : 1. A (2 mmol), DBDMH (1 mmol), tetrakis(triphenyl-phosphine)palladium(0) (100 mg), and copper(I) iodide (40 mg) were dissolved in a mixture of toluene (7 mL) and Et_3N (7 mL) under nitrogen gas protection. The mixture was heated to 50 °C with rapid agitation for 2.5 h. After removing the agitation device the reaction system was heated to 80 °C for 72 h. The post-processing step is the same as above.

The CMP powder was ground into very fine particles, which were evenly dispersed in toluene with the specific proportion of A, B glue (DOW CORNING) under ultrasound. The sponge was soaked in the solution and deposited for 2 h at 80 °C.

Antibacterial activity of hydantoin-based CMPs

Escherichia coli (*E. coli*, Gram-negative) and *Staphylococcus aureus* subsp. *aureus* (*S. aureus*, Gram-positive) were used as model microorganisms to challenge the antibacterial functions of the samples. The concentrations of *Escherichia coli* and *Staphylococcus aureus* were 10^6 to 10^7 CFU mL^{-1}.

A known amount of CMPH (5 mg) was dispersed in sterilized distilled water (10 mL), the mixture was vortexed and sonicated for 20 min. Then, 10 μL of the bacteria suspension was added into the CMPH-containing suspension with vortexing for 3 min. The resultant mixture was under constant shaking for 60 min at 37 °C to inhibit bacteria growth. Whereafter, the mixture (50 μL) was removed with a pipette to broth solutions (LB broth for *E. coli* and *S. aureus*), which were shaken overnight for culturing bacteria at 37 °C and 30 °C, respectively. Ultimately, the optical density (OD) value, which is an index reflecting the growth status of bacteria, was measured to detect the growth of bacteria with UV-vis and calculate the antibacterial efficiency.

A coliform plate count method was adopted to evaluate the antibacterial efficiency of CMPH. The antibacterial process was the same as above, and the mixture was coated on the solid broth to culture for 24 h at 37 °C and 30 °C. The numbers of colonies on the plates were counted, and the differences between the monomer and polymers were compared.

Characterization

Solid-state ^{13}C cross-polarization magic angel spinning (CP/MAS) NMR spectra were measured and recorded by a Bruker AVANCE III 400 MHz NMR spectrometer at a resonance frequency of 100.6 MHz. Fourier transform infrared spectroscopy (FTIR) spectra were collected from a range of 4000–400 cm^{-1} using a Mexus 670 spectra instrument. UV-vis absorption spectra were determined on an Agilent UV-Cary 5000 spectrophotometer. Thermal stability of the resulting polymers was evaluated by a thermogravimetric analyser (PerkinElmer). The samples were heated at a rate of 10 °C min^{-1} under protection of nitrogen. The porous structures of the materials were characterized with nitrogen isotherms measured at 77 K using a pore and surface analyzer (ASAP 2020 apparatus). A scanning electron microscope (SEM, JSM-6701F and JSM-6700F, JEOL, Ltd.) was used to identify the morphologies of CMPH. The efficiency of antibacterial was measured by UV-2102 PC.

Conclusions

In summary, we have demonstrated a new approach for creating novel CMPs-based bacteriostatic agents by covalently introducing hydantoin groups into the skeleton of CMPs networks through a simple palladium-catalyzed Sonogashira–Hagihara cross-coupling reaction. Two CMPH samples show high specific surface areas of 1411 $m^2 g^{-1}$ and 549 $m^2 g^{-1}$ with micrometer-sized particles and nanometer-sized fibers morphologies. These CMPH samples show high antibacterial activity and can completely inhibit the growth of bacteria at a 100 ppm dispersion concentration in 120 min. Interestingly, the CMPH can not only be fabricated as a monolithic nanoporous foam, but also can be loaded on the surface of diverse porous substrates such as filter paper, cloths, and even sponge to fabricate various cost-efficient antibacterial agents. The findings obtained from this study show the great potential of as-synthesized CMPH for efficient sterilization of water. In addition, based on their inherent physicochemical robustness, tunable porous structure, and especially designable flexibility, novel CMPs-based antibacterial agents could be anticipated and possibly designed by facile introduction of diverse antibacterial substituents into CMPs building blocks followed by a simple one-pot reaction, which may open a new opportunity for development of high performance antibacterial agents for water cleanness to address severe environmental issues.

Author contributions

Lihua Chen and An Li designed the research; Fei Wang, Feng Ren and Peng Mu synthesized the polymers; Fei Wang and Dan Ma performed bacteriostatic test; Fei Wang, Huijuan Wei and Chaohu Xiao performed samples characterization; Zhaoqi Zhu, Hanxue Sun, Weidong Liang performed data analysis and theoretical investigation; Jixiang Chen contributed important suggestions. All authors co-wrote the manuscript.

Conflicts of interest

There are no conflicts to declare.

Acknowledgements

The authors are grateful to the National Natural Science Foundation of China (Grant No. 51663012, 51462021, 51403092, 41361070 and 31272694), the Natural Science Foundation of

Gansu Province, China (Grant No. 1610RJYA001), Support Program for Hongliu Young Teachers (Q201411), Hongliu Elitist Scholars of LUT (J201401), Support Program for Longyuan Youth and Fundamental Research Funds for the Universities of Gansu Province and Program for Young Talent of State Ethnic Affairs Commission ([2016]57).

References

1 S. Binder, A. M. Levitt, J. J. Sacks and J. M. Hughes, *Science*, 1999, **284**, 1311–1313.
2 E. Larson and R. N. Olmsted, *Am. J. Infect. Control*, 2001, **29**, 69–72.
3 A. N. Neely and M. P. Maley, *J. Clin. Microbiol.*, 2000, **38**, 724–726.
4 E. Scott and S. F. Bloomfield, *J. Appl. Microbiol.*, 1990, **68**, 271–278.
5 M. J. Richards, J. R. Edwards, D. H. Culver and R. P. Gaynes, *Crit. Care Med.*, 1999, **27**(5), 887–892.
6 W. Litsky, *Am. J. Public Health*, 1990, **80**(1), 13–15.
7 H. Pionke and D. Glotfelty, *Water Res.*, 1989, **23**, 1031–1037.
8 S. D. Worley, D. Williams and R. A. Crawford, *Crit. Rev. Environ. Sci. Technol.*, 1988, **18**, 133–175.
9 A. Tijsma, H. J. Thibaut, D. Franco, D. Kai and J. Neyts, *Antiviral Res.*, 2016, **133**, 106–109.
10 Z. Chen and Y. Sun, *Ind. Eng. Chem. Res.*, 2006, **45**, 2634–2640.
11 S. Liu, T. H. Zeng, M. Hofmann, E. Burcombe, J. Wei, R. Jiang, J. Kong and Y. Chen, *ACS Nano*, 2011, **5**, 6971–6980.
12 W. Hu, C. Peng, W. Luo, M. Lv, X. Li, D. Li, Q. Huang and C. Fan, *ACS Nano*, 2010, **4**, 4317–4323.
13 O. Akhavan and E. Ghaderi, *ACS Nano*, 2010, **4**, 5731–5736.
14 C. D. Vecitis, K. R. Zodrow, S. Kang and M. Elimelech, *ACS Nano*, 2010, **4**, 5471–5479.
15 S. Kang, M. Herzberg, D. F. Rodrigues and M. Elimelech, *Langmuir*, 2008, **24**, 6409–6413.
16 E. R. Kenawy and A. G. Mahmoud, *Macromol. Biosci.*, 2003, **3**, 107–116.
17 A. Dong, Y.-J. Wang, Y. Gao, T. Gao and G. Gao, *Chem. Rev.*, 2017, **117**, 4806–4862.
18 Y. Sun and G. Sun, *J. Polym. Sci., Part A: Polym. Chem.*, 2001, **39**, 3348–3355.
19 S. D. Worley, F. Li, R. Wu, J. Kim, C. I. Wei, J. F. Williams, J. R. Owens, J. D. Wander, A. M. Bargmeyer and M. E. Shirtliff, *Surf. Coat. Int., Part B*, 2003, **86**, 273–277.
20 Y. Sun and G. Sun, *Phytother. Res.*, 1998, **12**, 163–166.
21 D. Delong, K. Gerzon and C. Ryan, Method of virus suppression by hydantoins, *U.S. Pat.*, No. 3,790,673, 1974.
22 L. M. Vance, N. Moscufo, M. Chow and B. A. Heinz, *J. Virol.*, 1997, **71**, 8759–8765.
23 D. J. Barton and J. B. Flanegan, *J. Virol.*, 1997, **71**, 8482.
24 E. Wessels, D. Duijsings, R. A. Notebaart, W. J. Melchers and F. J. van Kuppeveld, *J. Virol.*, 2005, **79**, 5163.
25 H. Toyoda, D. Franco, K. Fujita, A. V. Paul and E. Wimmer, *J. Virol.*, 2007, **81**, 10017.
26 M. Launay, D. Potin, M. J. B. Maillet, E. A. Nicolai, T. M. Dhar and E. J. Iwanowicz, Hydantoin compounds useful as anti-inflammatory agents, *U.S. Pat.*, No. 6,710,064, 2004.
27 R. A. Goodnow Jr and K. Le, Hydantoin-containing glucokinase activators, *U.S. Pat.*, No. 6,583,288, 2003.
28 Q. Sun and D. Kyle, Aryl substituted hydantoin compounds and their use as sodium channel blockers, *U.S. Pat.*, Application No. 10/630,814, 2003.
29 O. M. Yaghi, H. Li, C. Davis, D. Richardson and T. L. Groy, *ChemInform*, 1998, **29**, 474–484.
30 S. S. Han, H. Furukawa, O. M. Yaghi and G. W. Rd, *J. Am. Chem. Soc.*, 2008, **130**, 11580–11581.
31 X. Feng, X. Ding and D. Jiang, *Chem. Soc. Rev.*, 2012, **41**, 6010–6022.
32 S. Y. Ding and W. Wang, *Chem. Soc. Rev.*, 2013, **42**, 548–568.
33 C. D. Wood, B. Tan, A. Trewin, H. Niu, D. Bradshaw, M. J. Rosseinsky, Y. Z. Khimyak, N. L. Campbell, R. Kirk and A. Ev Stöckel, *Chem. Mater.*, 2007, **19**, 2034–2048.
34 J. X. Jiang, C. Wang, A. Laybourn, T. Hasell, R. Clowes, Y. Z. Khimyak, J. Xiao, S. J. Higgins, D. J. Adams and A. I. Cooper, *Angew. Chem., Int. Ed.*, 2011, **50**, 1072–1075.
35 B. Bonillo, R. S. Sprick and A. I. Cooper, *Chem. Mater.*, 2016, **28**, 3469–3480.
36 F. Goettmann, A. Fischer, M. Antonietti and A. Thomas, *Angew. Chem., Int. Ed.*, 2006, **45**, 4467–4471.
37 P. Kuhn, M. Antonietti and A. Thomas, *Angew. Chem., Int. Ed.*, 2008, **47**, 3450–3453.
38 N. Chaoui, M. Trunk, R. Dawson, J. Schmidt and A. Thomas, *Chem. Soc. Rev.*, 2017, **46**, 3302–3321.
39 D. He, D. S. He, J. Yang, Z. N. Low, R. Malpassevans, M. Carta, N. B. Mckeown and F. Marken, *ACS Appl. Mater. Interfaces*, 2016, **8**, 22425–22430.
40 C. Gu, N. Huang, J. Gao, F. Xu, Y. Xu and D. Jiang, *Angew. Chem., Int. Ed.*, 2014, **53**, 4850–4855.
41 L. Chen, Y. Yang and D. Jiang, *J. Am. Chem. Soc.*, 2010, **132**, 9138–9143.
42 Y. Xie, T. T. Wang, X. H. Liu, K. Zou and W. Q. Deng, *Nat. Commun.*, 2013, **4**, 1960.
43 X. Wang, K. Maeda, A. Thomas, K. Takanabe, G. Xin, J. M. Carlsson, K. Domen and M. Antonietti, *Nat. Mater.*, 2009, **8**, 76–80.
44 X. Feng, Y. Liang, L. Zhi, A. Thomas, D. Wu, I. Lieberwirth, U. Kolb and K. Müllen, *Adv. Funct. Mater.*, 2009, **19**, 2125–2129.
45 K. Wu, J. Guo and C. Wang, *Angew. Chem., Int. Ed.*, 2016, **55**, 6013–6017.
46 Y. Li, M. Liu and L. Chen, *J. Mater. Chem. A*, 2017, **5**, 13757–13762.
47 J.-X. Jiang, F. Su, A. Trewin, C. D. Wood, H. Niu, J. T. Jones, Y. Z. Khimyak and A. I. Cooper, *J. Am. Chem. Soc.*, 2008, **130**, 7710–7720.
48 R. Dawson, D. J. Adams and A. I. Cooper, *Chem. Sci.*, 2011, **2**, 1173–1177.
49 V. Gomez-Serrano, J. Pastor-Villegas, A. Perez-Florindo, C. Duran-Valle and C. Valenzuela-Calahorro, *J. Anal. Appl. Pyrolysis*, 1996, **36**, 71–80.

50 C. Su, R. Tandiana, B. Tian, A. Sengupta, W. Tang, J. Su and K. P. Loh, *ACS Catal.*, 2016, **6**, 3594–3599.
51 M. Thommes, K. Kaneko, A. V. Neimark, J. P. Olivier, F. Rodriguez-Reinoso, J. Rouquerol and K. S. Sing, *Pure Appl. Chem.*, 2015, **87**, 1051–1061.
52 X. Wei, Z. Wang, J. Chen, J. Wang and S. Wang, *J. Membr. Sci.*, 2010, **346**, 152–162.
53 A. Li, H.-X. Sun, D.-Z. Tan, W.-J. Fan, S.-H. Wen, X.-J. Qing, G.-X. Li, S.-Y. Li and W.-Q. Deng, *Energy Environ. Sci.*, 2011, **4**, 2062–2065.
54 Y. Chen, H. Sun, R. Yang, T. Wang, C. Pei, Z. Xiang, Z. Zhu, W. Liang and A. Li, *J. Mater. Chem. A*, 2015, **3**, 87–91.
55 L. Bao, H. Sun, Z. Zhu, W. Liang, P. Mu, J. Zang and A. Li, *Mater. Lett.*, 2016, **178**, 5–9.
56 F. Ren, Z. Zhu, X. Qian, W. Liang, P. Mu, H. Sun, J. Liu and A. Li, *Chem. Commun.*, 2016, **52**, 9797–9800.
57 X. Qian, Z.-Q. Zhu, H.-X. Sun, F. Ren, P. Mu, W. Liang, L. Chen and A. Li, *ACS Appl. Mater. Interfaces*, 2016, **8**, 21063–21069.
58 X. Qian, B. Wang, Z. Q. Zhu, H. X. Sun, F. Ren, P. Mu, C. Ma, W. D. Liang and A. Li, *J. Hazard. Mater.*, 2017, **338**, 224–232.
59 F. Wang, F. Ren, P. Mu, Z. Zhu, H. Sun, C. Ma, C. Xiao, W. Liang, L. Chen and A. Li, *J. Mater. Chem. A*, 2017, **5**, 11348–11356.
60 Y. Sun and G. Sun, *J. Appl. Polym. Sci.*, 2010, **80**, 2460–2467.
61 M. R. Avadi, A. M. M. Sadeghi, A. Tahzibi, K. H. Bayati, M. Pouladzadeh, M. J. Zohuriaan-Mehr and M. Rafiee-Tehrani, *Eur. Polym. J.*, 2004, **40**, 1355–1361.